

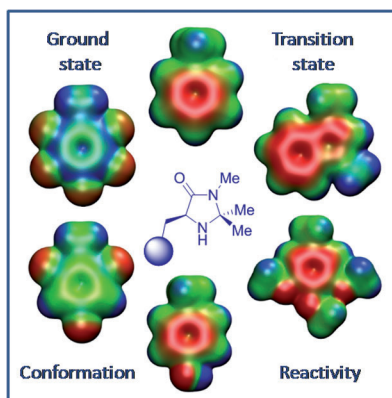
## Communications



### Catalyst Design

M. C. Holland, S. Paul, W. B. Schweizer,  
K. Bergander, C. Mück-Lichtenfeld,  
S. Lakhdar,\* H. Mayr,  
R. Gilmour\* ————— ■■■■-■■■■

Noncovalent Interactions in  
Organocatalysis: Modulating  
Conformational Diversity and Reactivity  
in the MacMillan Catalyst



**Intriguing imidazolidinones!** Inspired by noncovalent interactions in proteins, a series of electronically distinct MacMillan catalysts were designed. The effect of electronic modulation on ground state conformation, reactivity, and performance was studied in a catalytic setting with intriguing outcomes.

# Noncovalent Interactions in Organocatalysis: Modulating Conformational Diversity and Reactivity in the MacMillan Catalyst\*\*

Mareike C. Holland, Shyeni Paul, W. Bernd Schweizer, Klaus Bergander, Christian Mück-Lichtenfeld, Sami Lakhdar,\* Herbert Mayr, and Ryan Gilmour\*

Dedicated to Professor Dr. Jack D. Dunitz FRS on the occasion of his 90th birthday.

Organocatalysts are inimitable in both their structural mimicry of enzymatic systems and the activation modes by which they operate.<sup>[1]</sup> Much can be gleaned from studies of more complex, yet related, biomolecules and the noncovalent interactions that modulate their conformational dynamics and function.<sup>[2]</sup> Accordingly, the burgeoning field of organocatalysis is uniquely placed to benefit from the maturity of supramolecular and bio-organic chemistry,<sup>[3]</sup> and enantioselective catalysis to provide innovative solutions to long-standing problems in organic synthesis.<sup>[4]</sup> This juxtaposition facilitates the development of highly selective reactions proceeding via well-defined intermediates by direct application of stabilizing structural features that are well described in proteins; pertinent examples include CH- $\pi$  and  $\pi$ - $\pi$  interactions and hydrogen bond networks. Many of these quintessential characteristics are prominent in secondary amine organocatalysts; the phenylalanine-derived MacMillan catalyst (Figure 1) is an excellent example.<sup>[5]</sup> The iminium ensemble that is generated by the union of this imidazolidinone and an  $\alpha,\beta$ -unsaturated aldehyde exhibits the same CH- $\pi$ <sup>[6]</sup> and  $\pi$ - $\pi$  interactions<sup>[7]</sup> as those found in proteins. These intramolecular, noncovalent interactions have been detected spectroscopically and/or crystallographically, and validated by computation in a range of MacMillan-type iminium salts.<sup>[8,9]</sup> Particularly noteworthy is the propensity of

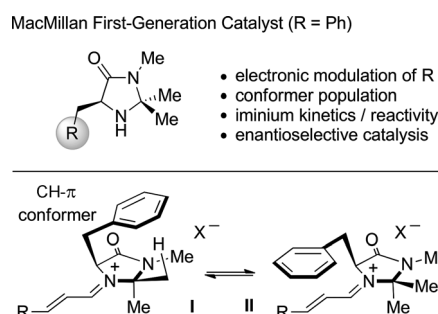


Figure 1. The first-generation imidazolidinone reported by MacMillan and co-workers in 2000.<sup>[5]</sup>

the phenylalanine side chain to participate in a CH- $\pi$  interaction with the *syn* methyl group of the catalyst core (I; Figure 1): this interaction is found ubiquitously in numerous enzyme structures.<sup>[6]</sup> Indeed, the system is geometrically predisposed to allow for it, making imidazolidinone-derived iminium salts valuable intermediates for fundamental physical organic studies of this type of interaction.<sup>[10]</sup> Moreover, there is ample support for a second low-energy conformation where the aryl ring shields the pendant iminium chain (II; Figure 1).<sup>[11]</sup> The role of these interactions in influencing conformation and reactivity in organocatalytic reactions requires clarification. Herein, we report the consequence of electronic modulation of the aromatic group on the conformation and reactivity of  $\alpha,\beta$ -unsaturated MacMillan-type iminium salts. The ground-state conformational studies are complemented by a reactivity and catalysis study, thus illustrating the importance of the aryl group electronics on catalyst performance.

The covalent nature of the organocatalytic intermediates allows for the isolation and characterization of these ensembles as part of the reaction design process. This notion of deconstructing reactions has been successfully applied on several occasions.<sup>[12]</sup> Initially, the iminium salts (1-6)-ClO<sub>4</sub><sup>-</sup> were prepared to generate a platform from which to begin this investigation, and synthesized from the constituent secondary amines and *trans*-cinnamaldehyde. The electronic nature of the aryl group is reflected by the component of the traceless quadrupole moment tensor orthogonal to the aromatic ring ( $Q_{zz}$ ) calculated for the corresponding toluene derivative (ArCH<sub>3</sub>) for simplicity (Figure 2; 2  $\rightarrow$  6,  $Q_{zz}$  3.01  $\rightarrow$  -5.68). In general, the addition of electron-withdrawing groups renders this number more positive, whilst electron-donating groups have the opposite effect. This can be clearly visualized by an

[\*] M. C. Holland, Dr. K. Bergander, Dr. C. Mück-Lichtenfeld, Prof. Dr. R. Gilmour  
Organisch Chemisches Institut  
Westfälische Wilhelms-Universität Münster  
Corrensstrasse 40, 48149 Münster (Germany)  
E-mail: ryan.gilmour@uni-muenster.de  
Homepage: <http://www.uni-muenster.de/Chemie.oc/gilmour/>

M. C. Holland, Dr. W. B. Schweizer  
Laboratorium für Organische Chemie  
ETH Zürich (Switzerland)

S. Paul, Prof. Dr. H. Mayr  
Department Chemie  
Ludwig-Maximilians-Universität München (Germany)

Dr. S. Lakhdar  
Laboratoire de Chimie Moléculaire et Thio-organique, ENSICAEN  
6 Boulevard Maréchal Juin, 14050 Caen (France)  
E-mail: sami.lakhdar@ensicaen.fr

[\*\*] We acknowledge generous financial support from the WWU Münster, the DFG (SFB 749), and the ETH Zürich (ETH Independent Investigator Research Award to R.G.).

Supporting information for this article is available on the WWW under <http://dx.doi.org/10.1002/anie.201301864>.

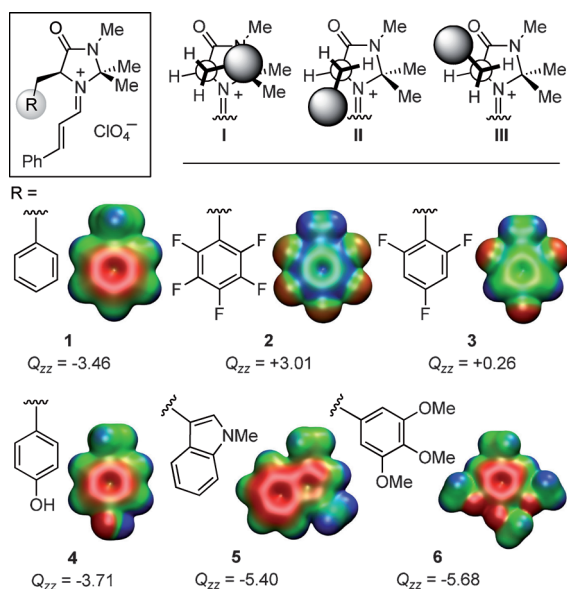


**Figure 2.** Top: Three possible low-energy conformers of iminium salt-derived  $\alpha,\beta$ -unsaturated iminium salts 1–6 (I = CH- $\pi$ ; II =  $\pi$ - $\pi$ ). Bottom: The components of the traceless quadrupole moment tensor orthogonal to the aromatic ring (Debye-Ångström,  $Q_{zz}$ ) are given for the corresponding toluene derivatives (i.e. ArCH<sub>3</sub>).  $Q_{zz}$  calculated using DFT (TPSS/def2-TZVP). Electrostatic potential maps (ESP) of the substituted toluene derivatives corresponding to 1–4, and 6 and the methyl indole derivative corresponding to 5. Isosurfaces correspond to an electron density of 0.005 a.u. Color range of the electrostatic potential: -0.02 (red) to +0.05 (blue).

electrostatic potential map (ESP) as shown in Figure 2. Gratifyingly, it was possible to isolate and crystallize an electron-deficient (2 ClO<sub>4</sub><sup>-</sup>, R = C<sub>6</sub>F<sub>5</sub>) and an electron-rich example (4 ClO<sub>4</sub><sup>-</sup>, R = C<sub>6</sub>H<sub>4</sub>OH) to compare solid-state conformations with that of 1.<sup>[9f]</sup>

The effect of electronic modulation was immediately evident on the conformation. Of the three staggered conformations indicated in Figure 2 (I–III), the electron-rich phenylalanine derivative 1 (R = Ph) resided in conformation I, a trend that was preserved in the tyrosine derivative 4 (R = C<sub>6</sub>H<sub>4</sub>OH; Figure 3, right).<sup>[13]</sup> In contrast, the electron-defi-

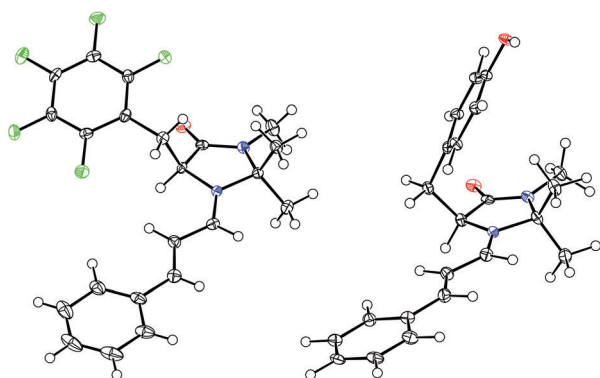


**Figure 3.** X-ray crystal structures of iminium salts 2 (conformer III) and 4 (conformer I). Thermal ellipsoids shown at the 50% probability level; the ClO<sub>4</sub><sup>-</sup> counterions have been omitted for clarity; gray C, green F, blue N, red O.<sup>[13,14]</sup>

cient pentafluorophenyl analogue 2 (R = C<sub>6</sub>F<sub>5</sub>) adopted conformation III (Figure 3, left) such that the aryl group lies proximal to the C=O unit of the imidazolidinone ( $\varphi_{CCCC} = +31^\circ$ ).<sup>[14]</sup> Houk and co-workers calculated the staggered conformer corresponding to III (crotonaldehyde derivative when R = Me, 1)<sup>[11]</sup> to be energetically unfavorable. Moreover, Seebach and Grimme have calculated that this species is not an energy minimum at all in their “windshield-wiper model”.<sup>[15]</sup> To the best of our knowledge structural data for systems with this conformation have so far not been reported.

To complement this crystallographic study, a detailed spectroscopic investigation was performed, including a conformer population analysis. The mole fractions ( $X_I$ ,  $X_{II}$ , and  $X_{III}$ ) of the electron-rich species 1 and 4–6, and the electron-deficient systems 2 and 3 were derived from the <sup>3</sup>J coupling constants (ArCH<sub>2</sub> and 5-H) using the Diez–Altona–Donders equation<sup>[16]</sup> with the aid of MestReJ v1.1.<sup>[17]</sup> It was assumed that only staggered rotamers with dihedral angles of 60° contribute to <sup>3</sup>J (I–III, Table 1). From this analysis it is evident

**Table 1:** Conformational analysis of 1–6; calculation of the mole fractions  $X_I$ ,  $X_{II}$ , and  $X_{III}$  at room temperature in MeCN.<sup>[a]</sup>

Iminium salt	$Q_{zz}$	Mole fractions			$\Delta\delta_{(syn/anti)}^{13C}$	
		$X_I$	$X_{II}$	$X_{III}$	<sup>1</sup> H	<sup>13</sup> C
2	+3.01	0.37	0.16 <sup>[b]</sup>	0.47 <sup>[b]</sup>	-0.13	+0.36
3	+0.26	0.39	0.21 <sup>[c]</sup>	0.40 <sup>[c]</sup>	-0.18	+0.06
1	-3.46	0.75	0.03	0.23	-0.89	-2.77
4	-3.71	0.76	0.04	0.20	-0.78	-2.48
5	-5.40	0.57	0.28	0.15	-0.58	-1.68
6	-5.68	0.65	0.17	0.18	-0.62	-1.87

[a] NMR spectra were recorded on an Agilent DD2 500 or 600 MHz spectrometer (room temperature, MeCN). The benzylic protons were individually assigned by NOE analysis. [b, c] Due to the absence of a significant HF heteronuclear NOE these values could be interchanged ( $X_{II} + X_{III} \approx 60\%$ ).

that electron-rich species such as 1, 4, 5, and 6 predominantly populate conformer I at room temperature. The remaining 25–40% are divided between II and III. Notably, in more electron-rich species such as 5 and 6 conformer II is populated more by 28% and 17%, respectively. In the parent system 1, conformer II is essentially unpopulated at rt. As expected, the electron-deficient pentafluorophenyl system 2 does not predominantly populate conformation I at room temperature, but instead shows a more varied distribution favoring II and III (roughly 60% overall). This tendency is preserved in species 3. These trends can also be derived from the <sup>1</sup>H and <sup>13</sup>C chemical shifts of the *gem*-dimethyl groups of these iminium salts (Table 1, right). Whilst the large  $\Delta\delta_{(syn/anti)}$  values in the <sup>1</sup>H NMR spectra of iminium salts 1 and 4–6 ( $\Delta\delta = 0.58$ – $0.89$  ppm) can be attributed to the shielding of the *syn*-methyl protons in conformer I, the small  $\Delta\delta_{(syn/anti)}$  values in 2 and 3 are indicative of the small population of

conformer **1** in these electron-deficient species. Similar conclusions can also be drawn from the  $^{13}\text{C}$  NMR spectra.

In order to examine how the electronic nuances of the aryl groups influence the electrophilic reactivities of the iminium salts, we have studied the kinetics of the reactions of the most electron-deficient (**2**) and the most electron-rich (**6**) species with ketene acetals **7** and **8**, which have previously been employed as reference nucleophiles. Previous work has established that the reactions of carbocations and Michael acceptors with  $\sigma$ ,  $n$ , and  $\pi$  nucleophiles follow Equation (1), in

$$\log k_2 (20^\circ\text{C}) = s_N (E + N) \quad (1)$$

which electrophiles are described by  $E$  (electrophilicity parameter) and nucleophiles are described by  $N$  (nucleophilicity parameter) and  $s_N$  (nucleophile-specific sensitivity parameter).<sup>[18]</sup>

Using this approach it has been possible to establish comprehensive electrophilicity and nucleophilicity scales covering more than 30 orders of magnitude. Recently, the reactivities of imidazolidinone-derived iminium salts have been shown to fit Equation (1) perfectly.<sup>[19]</sup> Now, the kinetics of the reactions of **2** and **6** with silyl ketene acetals **7** and **8** were followed photometrically in  $\text{CH}_2\text{Cl}_2$  at  $20^\circ\text{C}$  by monitoring the decay of the absorbances of **2** and **6** at 376 nm and 374 nm, respectively.

By using the nucleophiles **7** and **8** in large excess, pseudo-first-order kinetics were achieved, and the first-order rate constants  $k_{\text{obs}}$  ( $\text{s}^{-1}$ ) were derived from the exponential decays of the iminium salts **2** and **6** (Figure 4). Plots of  $k_{\text{obs}}$  versus the

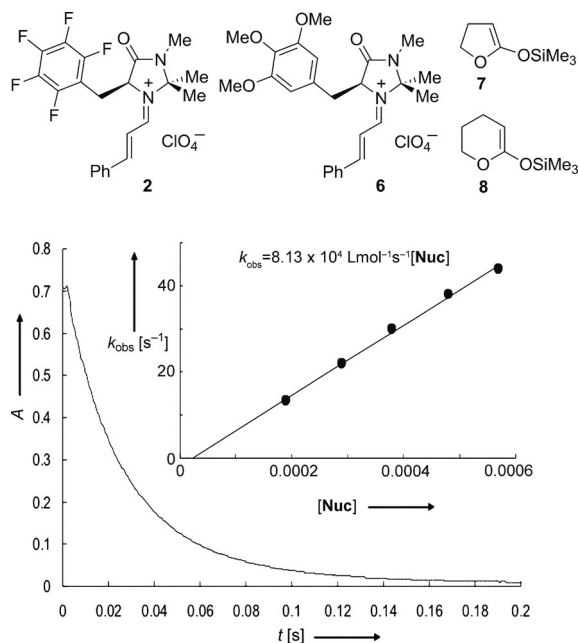


**Figure 4.** Exponential decay of the absorbance at 376 nm during the reaction of **6**  $\text{ClO}_4^-$  ( $9.55 \times 10^{-6} \text{ M}$ ) with **7** ( $5.70 \times 10^{-4} \text{ M}$ ). Inset: Determination of the second-order rate constant  $k_2$  from the dependence of the first-order rate constant  $k_{\text{obs}}$  for the reaction of **2**  $\text{ClO}_4^-$  with **7** on the concentration of ketene acetal **7** ( $20^\circ\text{C}$  in  $\text{CH}_2\text{Cl}_2$ ). Nuc = nucleophile.

**Table 2:** Second-order rate constants  $k_2$  for the reactions of the iminium salts **1**, **2**, and **6** with the ketene acetals **7** and **8** ( $20^\circ\text{C}$ ,  $\text{CH}_2\text{Cl}_2$ , counterion:  $\text{ClO}_4^-$ ).

	$k_2$ ( <b>7</b> ) [ $\text{M}^{-1} \text{s}^{-1}$ ]	$k_2$ ( <b>8</b> ) [ $\text{M}^{-1} \text{s}^{-1}$ ]	$E^{\text{[a]}}$
<b>1</b> <sup>[b]</sup>	$9.06 \times 10^3$	$5.23 \times 10^2$	$-7.2^{\text{[c]}}$
<b>2</b>	$8.13 \times 10^4$	$3.43 \times 10^3$	$-6.0$
<b>6</b>	$1.49 \times 10^4$	$5.78 \times 10^2$	$-7.0$

[a] The  $E$  parameters for **2** and **6** were determined from a least-squares minimization of  $\Delta^2 = \sum (\log k_2 - s_N(E+N))^2$  which uses the second-order rate constants  $k_2$  (this table) and the nucleophile parameters  $N$  and  $s_N$  (for **7**:  $N = 12.56$ ,  $s_N = 0.70$ ; for **8**:  $N = 10.61$ ,  $s_N = 0.86$ ).<sup>[18]</sup> [b]  $\text{OTf}^-$  counterion [c] Ref. [19a].

concentrations of the nucleophiles (Figure 4) were linear, with the second-order rate constants  $k_2$  ( $\text{M}^{-1} \text{s}^{-1}$ ) as slopes. The electrophilicity parameters (Table 2) show that **2** is about 9 times more reactive than **6**, exhibiting comparable reactivity to that of the iminium salt derived from MacMillan's second-generation catalyst (Figure 5).

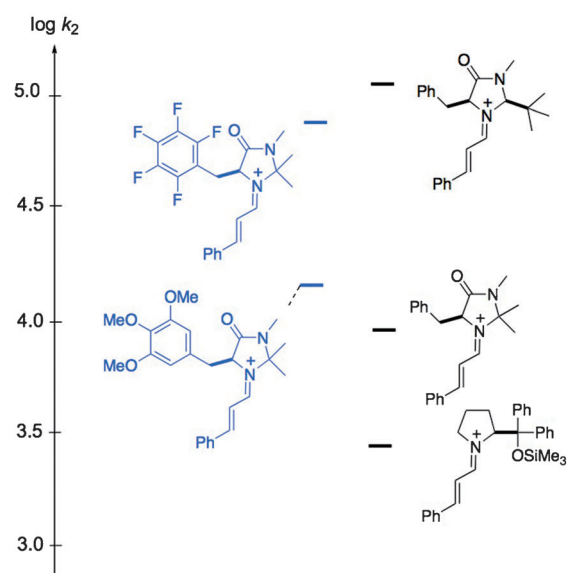


**Figure 5.** Comparison of the relative second-order rate constants for the reactions of the iminium ions **2** and **6** with the ketene acetal **7** in  $\text{CH}_2\text{Cl}_2$  at  $20^\circ\text{C}$ . The second-order rate constant for the reaction of the iminium ion derived from MacMillan's second-generation catalyst with the ketene acetal **7** is taken from Ref. [19b].

However, the presence of three methoxy groups at the phenyl ring of the imidazolidinone had little effect on the electrophilicity of the iminium system; the reactivity profile of **6** was comparable to that of MacMillan's first-generation catalyst (Figure 5).

Finally, to explore the behavior of the modified imidazolidinones in catalysis, the Friedel-Crafts reaction of  $N$ -methylpyrrole (**9**) with *trans*-cinnamaldehyde (**10**) was examined (Figure 6).<sup>[20]</sup> To this end, only the substituted benzene derivatives were screened for direct comparison of substituent effects. Reactions were performed in  $\text{THF}/\text{H}_2\text{O}$  at ambient temperature, using 20 mol% catalyst loading, and



- [10] M. Nishio, M. Hirota, Y. Umezawa, *The CH/π Interaction: Evidence, Nature and Consequences*, Wiley-VCH, Weinheim, **1998**.
- [11] R. Gordillo, J. Carter, K. N. Houk, *Adv. Synth. Catal.* **2004**, *346*, 1175–1185.
- [12] For examples from this laboratory see: C. Sparr, W. B. Schweizer, H. M. Senn, R. Gilmour, *Angew. Chem.* **2009**, *121*, 3111–3114; *Angew. Chem. Int. Ed.* **2009**, *48*, 3065–3068, and references [9f] and [11].
- [13] 925388 contains the supplementary crystallographic data for this paper. These data can be obtained free of charge from The Cambridge Crystallographic Data Centre via [www.ccdc.cam.ac.uk/data\\_request/cif](http://www.ccdc.cam.ac.uk/data_request/cif).
- [14] 925387 contains the supplementary crystallographic data for this paper. These data can be obtained free of charge from The Cambridge Crystallographic Data Centre via [www.ccdc.cam.ac.uk/data\\_request/cif](http://www.ccdc.cam.ac.uk/data_request/cif).
- [15] D. Seebach, U. Grošelj, W. B. Schweizer, S. Grimme, C. Mück-Lichtenfeld, *Helv. Chim. Acta* **2010**, *93*, 1–16.
- [16] a) C. Altona in *Encyclopedia of NMR* (Eds.: D. M. Grant, R. Morris), Wiley, New York, **1996**; b) E. Díez, J. San-Fabián, J. Guilleme, C. Altona, L. A. Donders, *Mol. Phys.* **1989**, *68*, 49–63.
- [17] A. Navarro-Vazquez, J. C. Cobas, F. J. Sardina, *J. Chem. Inf. Comput. Sci.* **2004**, *44*, 1680–1685.
- [18] H. Mayr, T. Bug, M. F. Gotta, N. Hering, B. Irrgang, B. Janker, B. Kempf, R. Loos, A. R. Ofial, G. Remennikov, H. Schimmel, *J. Am. Chem. Soc.* **2001**, *123*, 9500–9512.
- [19] a) S. Lakhdar, T. Tokuyasu, H. Mayr, *Angew. Chem.* **2008**, *120*, 8851–8854; *Angew. Chem. Int. Ed.* **2008**, *47*, 8723–8726; b) S. Lakhdar, J. Ammer, H. Mayr, *Angew. Chem.* **2011**, *123*, 10127–10130; *Angew. Chem. Int. Ed.* **2011**, *50*, 9953–9956; c) H. Mayr, S. Lakhdar, B. Maji, A. R. Ofial, *Beilstein J. Org. Chem.* **2012**, *8*, 1458–1478.
- [20] N. A. Paras, D. W. C. MacMillan, *J. Am. Chem. Soc.* **2001**, *123*, 4370–4371.
- [21] S. Lakhdar, H. Mayr, *Chem. Commun.* **2011**, *47*, 1866–1868.
- [22] J. F. Austin, D. W. C. MacMillan, *J. Am. Chem. Soc.* **2002**, *124*, 1172–1173.
- [23] a) J. C. Ma, D. A. Dougherty, *Chem. Rev.* **1997**, *97*, 1303–1324; b) J. P. Gallivan, D. A. Dougherty, *Proc. Natl. Acad. Sci. USA* **1999**, *96*, 9459–9464; c) L. M. Salonen, M. Ellermann, F. Diederich, *Angew. Chem.* **2011**, *123*, 4908–4944; *Angew. Chem. Int. Ed.* **2011**, *50*, 4808–4842.
- [24] Y. Mori, S. Yamada, *Molecules* **2012**, *17*, 2161–2168.